Carbohydrate Polymers 314 (2023) 120900

Contents lists available at ScienceDirect

Carbohydrate Polymers

journal homepage: www.elsevier.com/locate/carbpol

Hyaluronan-estradiol nanogels as potential drug carriers to target ER+ breast cancer cell line

L. Paoletti [a], N. Zoratto [a], M. Benvenuto [b,c], D. Nardozi [d], V. Angiolini [d], P. Mancini [d], L. Masuelli [d], R. Bei [c], G.V. Frajese [e], P. Matricardi [a], M. Nalli [a], C. Di Meo [a,*]

[a] Department of Drug Chemistry and Technologies, Sapienza University of Rome, P.le A. Moro 5, 00185 Rome, Italy
[b] Saint Camillus International, University of Health and Medical Sciences, Via di Sant'Alessandro 8, 00131 Rome, Italy
[c] Department of Clinical Sciences and Translational Medicine, University of Rome "Tor Vergata", Via Montpellier 1, 00133 Rome, Italy
[d] Department of Experimental Medicine, Sapienza University of Rome, Viale Regina Elena 324, 00161 Rome, Italy
[e] Department of Sports Science, Human and Health, University of Rome 'Foro Italico', Piazza Lauro De Bosis, 15, 00135 Rome, Italy

ARTICLE INFO

Keywords:
Hyaluronan
Estradiol
Drug delivery
Nanohydrogels
Active targeting
Breast cancer

ABSTRACT

An innovative hyaluronan-based nano-delivery system is proposed for the active targeting towards ER+ breast cancer. Hyaluronic acid (HA), an endogenous and bioactive anionic polysaccharide, is functionalized with estradiol (ES), a sexual hormone involved in the development of some hormone-dependent tumors, to give an amphiphilic derivative (HA-ES) able to spontaneously self-assemble in water to form soft nanoparticles or *nanogels* (NHs). The synthetic strategy used to obtain the polymer derivatives and the physico-chemical properties of the obtained nanogels (ES-NHs) are reported. ES-NHs ability to entrap hydrophobic molecules has also been investigated, by loading curcumin (CUR) and docetaxel (DTX), both able to inhibit the growth of ER+ breast cancer. The formulations are studied for their capability to inhibit the growth of the MCF-7 cell line, thus evaluating their efficacy and potential as a selective drug delivery systems. Our results demonstrate that ES-NHs have not toxic effects on the cell line, and that both ES-NHs/CUR and ES-NHs/DTX treatments inhibit MCF-7 cell growth, with ES-NHs/DTX effect higher than that of free DTX. Our findings support the use of ES-NHs to deliver drugs to ER+ breast cancer cells, assuming a receptor-dependent targeting.

1. Introduction

The delivery of bioactive molecules to the target site has attracted increasing attention over the past three decades as a turning point in the treatment of several diseases (Mazdaei & Asare-Addo, 2022). In fact, the traditional drug use can be quite challenging, as it is often characterized by limited efficacy, inefficient biodistribution, lack of selectivity and numerous side effects (Senapati, Mahanta, Kumar, & Maiti, 2018). These drawbacks can be overcome by controlling and targeting the delivery of bioactive molecules using the so-called drug delivery systems (DDS) (Vargason, Anselmo, & Mitragotri, 2021). Among them, the nano-DDS turn out to be the most promising, due to their ability to: (a) modify the pharmacokinetics and biodistribution of the cargo; (b) act as a reservoir for prolonged drug release; (c) avoid rapid degradation or clearance of the drug; (d) increase the drug concentration at the target site, thus reducing the number of doses required for therapy with less side effects (Patra et al., 2018). Small molecules, peptides, proteins, and nucleic acids can be loaded into nanoparticle systems (NPs), which can be functionalized on the surface to escape opsonization by the immune system: when specific ligands are linked to the NPs surface, they can actively deliver the cargo to cells that have receptors capable of selectively recognizing the ligand. Furthermore, these systems are able to accumulate preferentially in tumor or inflamed tissues, which are characterized by highly permeable endothelia and poor lymphatic

Abbreviations: 17-ES-Br, (17β)-Estradiol-bromobutyrate; ABTS, 2,2′-azino-bis(3-ethybenzothiazoline-6-sulfonic acid); CUR, curcumin; CvME, caveola-mediated endocytosis; DAPI, 4′,6-diamidino-2-phenylindole; DD, derivatization degree; DDS, drug delivery systems; %DL, drug loading; DMEM, Dulbecco's modified Eagle's medium; DTX, docetaxel; %EE, encapsulation efficiency; ES, estradiol; ES-NHs, estradiol-nanohydrogels; HA, hyaluronic acid; HA-CH, hyaluronan-cholesterol; HA-ES, hyaluronan-estradiol; HA-Rfv, hyaluronan-riboflavin; mERs, membrane estrogen receptors; NHs, nanohydrogels; NMP, *N*-methyl-2-pyrrolidone; NPs, nanoparticles; RBA, relative binding affinity; Rhod, rhodamine B-isothiocyanate; SRB, sulforhodamine B; TEA, triethylamine; TEM, transmission electron microscopy.

* Corresponding author.
E-mail address: chiara.dimeo@uniroma1.it (C. Di Meo).

https://doi.org/10.1016/j.carbpol.2023.120900
Received 20 December 2022; Received in revised form 23 March 2023; Accepted 8 April 2023
Available online 13 April 2023

drainage (EPR effect – *enhanced permeability and retention effect*) (Sanità, Carrese, & Lamberti, 2020).

Polysaccharides have been widely investigated as ideal materials for NPs preparation thanks to their biocompatibility, biodegradability, low-toxicity and bioadhesion properties. Furthermore, polysaccharide-based NPs offer benefits in terms of high loading efficiency, rapid drug release rates and good targeting ability through the easy functionalization of the polymeric backbones (Plucinski, Lyu, & Schmidt, 2021).

Hyaluronic acid (HA) is one of the most investigated polysaccharides in the pharmaceutical field, especially in the development of DDS used in viscosupplementation, ophthalmology, pneumology, rhinology, urology and in anticancer therapy, as well as in cosmetics and aesthetic medicine (Fallacara, Baldini, Manfredini, & Vertuani, 2018). On a structural level, it can be defined by linear chains of disaccharide units linked by β-1,4 glycosidic bonds: each unit is composed of D-glucuronic acid and *N*-acetyl-glucosamine linked by β-1,3 glycosidic bond (Weissmann & Meyer, 1954). HA functionalization with small hydrophobic molecules leads to amphiphilic derivatives, which are able to spontaneously self-assemble in water through weak interactions that guide and promote aggregation (Curcio et al., 2022). When an optimum balance between the hydrophilic and hydrophobic moieties of the amphiphilic chains is reached, the rearrangement results in the formation of nanohydrogels or nanogels (NHs), which are defined as aqueous dispersions of hydrogel particles with a nanoscale size (Kabanov & Vinogradov, 2009). These nanosystems are highly versatile as they are able to encapsulate both hydrophilic and hydrophobic drugs. Moreover, molecules that are stable at high temperatures can be loaded at the same time of NHs formation, leading to sterile, and ready-to-use formulations in a single step (Zoratto et al., 2021).

NHs based on hyaluronan-cholesterol (HA-CH) and hyaluronan-riboflavin (HA-Rfv) have already been described in previous works (Di Meo et al., 2015; Montanari et al., 2013) aiming to exploit the interaction of HA with CD44 receptors – overexpressed on the surface of several solid tumors (Mattheolabakis, Milane, Singh, & Amiji, 2015) – which results in the internalization of the nanosystems (Montanari, Di Meo, Oates, Coviello, & Matricardi, 2018). However, the choice of a suitable hydrophobic ligand to graft onto the HA backbone may provide the system with new properties, selectivity to cancer cells and *in-situ* drug release. Indeed, estradiol (ES), an estrogen steroid hormone involved in the onset and growth of some types of cancer, could be a good choice. Since ES is involved both in the promotion of endothelial cell proliferation in the endometrium and in the stimulation of mammary glands growth, it plays a key role in the regulation of tumor growth in some endometrial, ovarian and breast cancer (Johansson et al., 2022; Khan, Uzair, Nazli, & Chen, 2022). It exerts its action by binding specific estrogen receptors, which are located in the nucleus (ERα and Erβ) or in the cell membrane (GPER1) (Fuentes & Silveyra, 2019). These receptors, together with progesterone and human epidermal growth factor 2 receptors (ErbB2/HER2), are markers for the classification of breast cancer into three major subtypes based on their presence or absence: ER+/HER2– (70 % of patients), HER2+ (15–20 %), and triple-negative (15 %) which is lacking in all markers (Waks & Winer, 2019). Recently, a new subpopulation of membrane estrogen receptors (mERs) has been identified as a result of a migration of a small pool of nuclear ERα and Erβ (Acconcia et al., 2021; Tecalco-Cruz, Macías-Silva, Ramírez-Jarquín, & Ramírez-Jarquín, 2022). These receptors are mainly placed in caveolaes and, following the ligand binding, they can be internalized *via* dynamin-dependent, caveola-mediated endocytosis (CvME) (Marczell et al., 2018; Paliwal, Paliwal, Agrawal, & Vyas, 2012). They have been detected on the membrane of cancer cells in breast tissue (Acconcia & Marino, 2011; Boonyaratanakornkit et al., 2018), while non-tumor breast tissue is negative at this receptor, suggesting their potential as a target for chemotherapeutic selective treatment (Kampa, Pelekanou, & Castanas, 2008; Paliwal et al., 2012). Moreover, since a CvME mechanism could enable internalization through a less destructive path, bypassing sorting to early endosomes and thus preventing fusion with lysosome, a sub-nuclear active targeting towards nuclear ERα and Erβ is also possible (Tammam, Azzazy, & Lamprecht, 2016). In this regard, surface functionalization of liposome, dendrimers and synthetic polymeric NPs with ES have already proved their efficacy in the site-specific delivery of chemotherapeutics to breast cancer cells (Jain, Spandana, Agrawal, Kushwah, & Thanki, 2015; Paliwal et al., 2012).

Curcumin (CUR), a pleiotropic polyphenol derived from the rhizome of *Curcuma longa*, is a multitarget drug showing antitumor, anti-inflammatory, antioxidant, immunomodulatory and antimicrobial activities targeting a variety of signal transduction pathways deregulated in tumors (Focaccetti et al., 2020; Giordano & Tommonaro, 2019).

Docetaxel (DTX) is a semi-synthetic taxane largely used as a first-line drug in chemotherapy for breast cancer. Several trials report that the combination of DTX with other chemotherapy drugs, such as Trastuzumab, correlates with a better outcome and overall survival of patients with metastatic breast cancer (Swain et al., 2020). DTX has the ability to inhibit the proliferation and induce apoptosis in cancer cells by phosphorylation of BCL-2 (Guo et al., 2022; Škubník, Pavlíčková, Ruml, & Rimpelová, 2021).

In the present study, ES molecules were grafted on HA chains by a double ester bond, with a range of derivatization degrees (HA-ES). Self-assembled and sterile nanogels (ES-NHs) were prepared by autoclave treatment of HA-ES aqueous dispersions and loaded with CUR or DTX during or after the NHs formation, respectively. With the aim to determine the ability of such nanosystems to interact with ES receptors, they were incubated with MCF-7 cell line. Results show that CUR-loaded NHs have similar effect to the free compound, while DTX-loaded ES-NHs are more active compared to the free drug, hence suggesting their potential efficacy as an active membrane targeting and nuclear delivery formulation in the treatment of breast cancer.

2. Materials and methods

2.1. Materials

2.1.1. Chemicals

Sodium hyaluronan HA^-Na^+ (Hysilk, $M_W = 1.15 \times 10^5$) was purchased from Contipro (Dolni Dobrouč, Czech Republic) and was exchanged in tetrabutylammonium salt (HA^-TBA^+) by using a Dowex resin. β-Estradiol (ES), 4-bromobutyryl chloride, acetonitrile (AcCN, HPLC grade ≥ 99.8 %), trifluoroacetic acid (TFA), phosphate buffered saline tablets (PBS), 2,2′-azino-bis(3-ethybenzothiazoline-6-sulfonic acid) (ABTS), potassium persulfate, sulforhodamine B (SRB), rhodamine B-isothiocyanate (Rhod) and glycerol were purchased from Sigma-Aldrich (Milan, Italy). Docetaxel (DTX) and curcumin (CUR) were purchased from Tokyo Chemical Industry (TCI).

Other chemicals were reagent grade and used without further purifications.

2.1.2. Cell line

Human breast cancer cells, MCF-7, obtained by ATCC (HTB-22™) were maintained in DMEM (Dulbecco's modified Eagle's medium) supplemented with 10 % fetal bovine serum, and 1 % antibiotics (100 U/mL penicillin and 100 μg/mL streptomycin). The cells were grown at 37 °C in a humidified incubator under 5 % CO_2 atmosphere.

2.2. Methods

2.2.1. Synthesis of (17β)-Estradiol-bromobutyrate (17-ES-Br)

17-Estradiol-bromobutyrate was synthesized by esterification of the aliphatic hydroxylic group of the hormone with 4-bromobutyryl chloride, in the presence of TEA. Specifically, 300 mg of ES (1.1 mmol; 1 meq) were dissolved in 6 mL of DMF and 307 μL of TEA (2.2 mmol, 2 meq) were then added. The mixture was magnetically stirred at room temperature for 30 min. Then, 255 μL of 4-bromobutyryl chloride (2.2 mmol, 2 meq) were added dropwise in 4 aliquots every 30 min.

The reaction was carried out under nitrogen atmosphere for 3 h from the latest addition. TLC was performed on Fluka silica gel (eluent cyclohexane/ethyl acetate 80:20) and then exposed to iodine (I_2) vapor. After that, the reaction mixture was poured into 110 mL of ethyl acetate and extracted five times with a 1/3 volume of aqueous phases. Specifically, it was washed with HCl 0.05 M, then with $NaHCO_3$ saturated solution, and three times with double-distilled water. The organic phase was then dried with anhydrous Na_2SO_4, desiccated under vacuum and purified by chromatography on silica gel 60. 17-ES-Br was eluted using a mobile phase composed of cyclohexane/ethyl acetate (90:10), dried and the yield of the reaction was finally calculated.

The collected products were analysed by infrared spectroscopy, using a FTIR Cary 630 spectrometer equipped with ATR system (Agilent Technologies, Santa Clara, California, US), and ^1H and ^{13}C nuclear magnetic resonance (NMR), using a Bruker Avance 400 spectrometer, by dissolving the first product in $CDCl_3$ and the second one in DMSO-d_6. Moreover, mass spectrometry (MS) experiments on 17-ES-Br product were performed using an AmaZon SL ion trap (Bruker Daltonics) equipped with an electrospray ionization source (ESI) operating in the positive ion mode, by dissolving it in 1:1 H_2O (2 % NaCl)/AcCN to the millimolar concentration.

2.2.2. Synthesis of hyaluronan-estradiol (HA-ES) derivatives

For the HA-ES synthesis, 200 mg of HA^-TBA^+ (323 μmol) were dissolved in 6.6 mL of NMP under magnetic stirring at room temperature. Then, a proper amount of 17-ES-Br, previously solubilized in 1 mL of NMP, was added to HA^-TBA^+ solution in order to obtain different stoichiometric derivatization degrees (moles of ES *per* moles of HA repeating unit) from 5 % to 70 %, as reported in table S1 (see Supplementary Material).

The reaction mixture was kept for 48 h at 38 °C under magnetic stirring. Thereafter, the sample was cooled at room temperature and 760 μL of a NaCl saturated solution (10 % of the sample volume) were added dropwise. The mixture was left under magnetic stirring for 30 min to allow the replacement of TBA^+ ions with Na^+ ions. The product was precipitated in acetone, left for 1 h at 4 °C, then the supernatant was withdrawn, and the product was dispersed in double-distilled water and dialysed (Visking Tubes, Cut-Off 12–14 kDa) against distilled water until a conductivity value <2 mS was reached. The obtained polymer was neutralized to pH 7.0 using NaOH 0.05 M and freeze-dried; the final reaction yield was up to 90–97 %. The product was stored at 25 °C, protected from moisture and light.

2.2.3. Evaluation of HA-ES derivatization degree

The derivatization degree (DD) of HA-ES was assessed for the derivatives with stoichiometric derivatization degrees of 40 % and 70 % ($HA\text{-}ES_{40}$ and $HA\text{-}ES_{70}$, respectively), by an alkaline hydrolysis of the ester bonds followed by the quantification of the free ES. Each derivative was dispersed in double-distilled water at a concentration of 0.5 mg/mL, the pH was adjusted to 13.0 by NaOH 10 M and then the mixture was sonicated for 30 min using a Starsonic 35 instrument (Liarre S.r.l., Casalfiumanese - BO, Italia). The suspension was left overnight under magnetic stirring at room temperature. It was further sonicated for 1 h, extracted 5 times with ethyl acetate, dried under vacuum and, finally, the hydrolysed ES was solubilized in 3 mL of AcCN (HPLC grade). ES quantification was performed by HPLC using a Knauer Azura instrument equipped with a binary pump (Azura P 6.1L) and a UV–Vis detector (190–750 nm, Azura UVD 2.1 L). The column used was a Knauer Eurospher II 100–5 C18 (4.6 × 250 mm) and all analyses were carried out at λ = 225 nm, using water/AcCN as mobile phase in gradient mode, from 50:50 up to 0:100, at a flowrate of 1 mL/min. A calibration curve was previously obtained with ES standard solutions in AcCN in the range of 15.63–500 μg/mL ($R^2 = 0.999$, $n = 5$).

The percentage of functionalization was calculated using the Eq. (1):

$$DD = \frac{\text{mol of ES}}{\text{mol of HANa repeating units}} \times 100 \quad (1)$$

2.2.4. Preparation and characterization of hyaluronic acid-estradiol nanogels (ES-NHs)

HA-ES derivatives were dispersed at 1 or 2 mg/mL in double-distilled water and left overnight under magnetic stirring at room temperature. Then, the suspensions were autoclaved at 121 °C, 1.1 bar for 20 min, using a Juno Liarre autoclave (230 VAC, 50/60 Hz, 12 A, 2000 W), leading to the formation of sterile ES-NHs by self-assembling (Montanari et al., 2015). ES-NHs size and polydispersity (PDI) were measured *via* Dynamic Light Scattering (DLS) using a Submicron Particle Sizer Autodilute Model 370 (Nicomp), controlled by the CW388 software program. *Z*-potential was measured using a Malvern NanoZetaSizer ZS90 dynamic light scattering instrument (Malvern Instruments, Worcestershire, United Kingdom), equipped with a 5 mW HeNe laser (λ = 632.8 nm). ES-NHs morphology was observed by transmission electron microscopy (TEM): ES-NHs (10 μL) were dropped on formvar–carbon-coated copper grids (EMS, PA, USA) and allowed to adsorb for 15 min. For negative staining the grids were stained with a 2 % uranyl acetate solution for 1 min at room temperature. Excess of staining solution was adsorbed by the filter paper and the grids were air-dried and observed with a TEM Philips Morgagni268D (FEI, Netherlands) at an accelerating voltage of 80 kV. Digital images were taken with Mega View imaging software (Quagliarini et al., 2021).

2.2.5. Formulation and characterization of curcumin-loaded nanogels (ES-NHs/CUR) and docetaxel-loaded nanogels (ES-NHs/DTX)

The encapsulation of CUR and DTX as hydrophobic molecules (logP = 3.2 and 4.1, respectively) into ES-NHs was achieved using the film forming technique. Stock solutions of CUR and DTX in acetone (2 mg/mL) were prepared and then 0.5 mL of each stock was transferred in a vial in order to have a total amount of drug equal to 1 mg. The organic solvent was then removed using a Heidolph Hei-VAP rotary evaporator (Buchi, Schwabach, Germany), obtaining a dry thin film of each molecule.

The loading procedure was then different for the two substances. For CUR loading, 3 mL of a HA-ES suspension (1 mg/mL) were added to the film and the sample was left under magnetic stirring at room temperature for 90 min in the dark, to prevent CUR photodegradation. Then the sample was autoclaved at 121 °C and 1.1 bar, for 20 min leading to the formation of loaded and sterile ES-NHs/CUR (Montanari et al., 2019). Instead, DTX was not subject to the standard autoclaving process due to its instability at high temperatures. For this reason, DTX film was hydrated with 3 mL of empty ES-NHs suspension (1 mg/mL), previously autoclaved, at 40 °C and under gentle magnetic stirring for 15 h.

At the end of the loading procedures, both formulations were purified by centrifugation (4000 rpm, 10 min) removing the unloaded drugs by precipitation; then ES-NHs/DTX were sonicated for 20 min, using an ultrasonic bath sonicator (Starsonic-35, Liarre), before assessing size, PDI and ζ-potential by DLS.

The determination of the amount of the drugs loaded into ES-NHs was carried out indirectly by quantification of residual CUR or DTX. Pellet obtained after centrifugation and remaining drugs in the films were solubilized in 5 mL of AcCN, filtered using a 0.2 μm Sartorius PTFE membrane, and injected into the HPLC. CUR samples were analysed by HPLC using a mobile phase composed by water (+ 0.1 % V/V of TFA)/acetonitrile (+ 0.1 % V/V of TFA) in gradient mode, from 50:50 to 0:100, at a flow-rate of 1 mL/min. DTX samples were analysed using a mixture of water (+ 0.1 % V/V of TFA)/acetonitrile (+ 0.1 % V/V of TFA) as eluent, in 40:60 isocratic mode and at a flow-rate of 1 mL/min. The molecules were detected by setting λ at 425 and 225 nm respectively, using two calibration curves previously obtained with CUR standard solutions in AcCN in the range of 0.39–50 μg/mL ($R^2 = 0.999$, $n = 8$) and DTX standard solutions in AcCN in the range of 7.81–500 μg/

mL ($R^2 = 0.999$, $n = 7$).

The amount of CUR or DTX entrapped into ES-NHs allowed the evaluation of the encapsulation efficiency (%EE) and of the drug loading percentage (%DL), using the Eqs. (2) and (3), respectively.

$$\%EE = \frac{\text{amount of loaded CUR or DTX (mg)}}{\text{amount of CUR or DTX used (mg)}} \times 100 \quad (2)$$

$$\%DL = \frac{\text{amount of loaded CUR or DTX (mg)}}{\text{amount of HAES derivative (mg)}} \times 100 \quad (3)$$

Stability of loaded ES-NHs, prepared as described above, was evaluated at 4 °C for 7 days in phosphate buffer 0.01 M (pH = 7.4) and glycerol 2 % w/V, miming physiological conditions. Moreover, empty and loaded ES-NHs were freeze-dried using a Lyovapor L-200 instrument (Buchi, Schwabach, Germany) working at −55 °C and at 0.2 mbar. Size and PDI values of both formulations were assessed before and after the freeze-drying process by re-dispersion in double-distilled water.

2.2.6. Antioxidant activity of ES-NHs/CUR in tube

Antioxidant activity of ES-NHs/CUR was evaluated by ABTS assay: a solution of radical cation $ABTS^{\bullet+}$ 7 mM in water was prepared approximately 14 h before the analysis by adding 88 μL of a potassium persulfate solution 38 mg/mL to 5 mL of ABTS solution 3.8 mg/mL. The stock solution was stored in the dark at room temperature and then diluted in order to have an absorbance (Abs) of 0.70 ± 0.02 at 730 nm. Experiments were performed with a Perkin-Elmer double beam "Lambda 3A" model Ultraviolet-Visible (UV–Vis) spectrophotometer set at "time drive" mode to display the decrease of the maximum absorption value over time at a certain wavelength. Analyses were carried out by adding 100 μL of ES-NHs/CUR suspensions (previously diluted 1:2) to 2.9 mL of the diluted $ABTS^{\bullet+}$ solution, as already reported (Montanari et al., 2019). For an appropriate comparison, ABTS assay was also tested on free CUR prepared at the same concentration as the reference samples. ES-NHs/CUR antioxidant activity (A) and its increase compared to free CUR (IA) were calculated at 6, 12 and 30 min by using the Eqs. (4) and (5).

$$\%A = \frac{\text{abs ABTS} - \text{abs sample}}{\text{abs ABTS}} \times 100 \quad (4)$$

$$\%IA = \frac{\text{A entrapped CUR} - \text{A free CUR}}{\text{A free CUR}} \times 100 \quad (5)$$

2.2.7. Sulforhodamine B (SRB) assay

Cells were seeded at 5×10^3 cells/well in 96-well plates and incubated at 37 °C to allow cell attachment. After 24 h, cells were incubated for 48 h with ES-NHs/CUR, ES-NHs and CUR (6–25 μM) or with DMSO (equivalent amount to that administered at the highest concentration of CUR), or with ES-NHs/DTX, ES-NHs and DTX (12.5–50 μM) or with DMSO (amount equivalent to that administered at the highest concentration of DTX). In both cases, empty ES-NHs were used at the same concentration needed for the treatments with ES-NHs/CUR 6 μM or 25 μM and with ES-NHs/DTX 12.5 μM or 50 μM. Cells were then fixed with cold trichloroacetic acid (final concentration 10 %) for 1 h at 4 °C. Afterwards, the assay was performed as previously described (Masuelli et al., 2012). Briefly, after four washes with distilled water, the plates were air-dried and stained for 30 min with 0.4 % (wt/V) SRB in 1 % acetic acid. After four washes with 1 % acetic acid to remove the unbound dye, the plates were air-dried and cell-bound SRB was dissolved with 200 μL/well of 10 mM unbuffered Tris Base solution. The optical density (O.D.) of the samples was determined at 540 nm using a spectrophotometric plate reader. The percentage survival of the cultures treated with ES-NHs/CUR, ES-NHs, CUR, ES-NHs/DTX, ES-NHs or DTX was calculated by normalization of their O.D. values to those of the control cultures treated with DMSO 0.01 % V/V (Benvenuto et al., 2021).

The experiments were performed in triplicate and repeated three times.

2.2.8. Internalization experiments

Synthesis of fluorescent NHs (Rhod-ES-NHs): $HA\text{-}ES_{40}$ derivative was dispersed in bi-distilled water at a concentration of 1.5 mg/mL and left under magnetic stirring overnight at room temperature. Then a stock solution of rhodamine B-isothiocyanate (Rhod) 9 mg/mL was prepared in DMSO and added to the samples: 8 μL *per* mg of polymer, corresponding to a theoretical functionalization degree of 6.0 % mol/mol. The reaction was left under magnetic stirring in the dark for 5 h at room temperature, dialysed against bi-distilled water and freeze-dried. The rhodaminated $HA\text{-}ES_{40}$ was then re-dispersed at a concentration of 1 mg/mL in bi-distilled water and autoclaved for 20 min at 121 °C and 1.1 bar to allow the formation of Rhod-ES-NHs. The nanosystems were finally freeze-died and stored at 4 °C in the dark.

Fluorescence analysis: 6×10^5 MCF-7 cells were seeded on 12 mm glass coverslips in a 24-well plate and allowed to adhere for 48 h. Then, cells were washed three times with PBS, and incubated in 1 mL of complete DMEM added with Rhod-ES-NHs (corresponding to a final concentration of 0.01 mg/ mL). Free Rhod was used as negative control.

After 30 min, medium was removed and cells were washed three times with PBS. Cells were fixed with 4 % (V/V) formaldehyde (1 mL, 10 min), washed three times with PBS, and incubated with Triton X-100 (0.1 %, V/V, 1 mL, 5 min). Cells were washed three times with PBS and nuclei were stained with 4′,6-diamidino-2-phenylindole (DAPI) reagent (1 μg/ mL, 1 mL for 1 min). Finally, cells were washed again and 5 μL Mowiol was added.

Fluorescence signal of Rhod-ES-NHs was analysed by recording stained images using an Axio Observer Z1 inverted microscope, equipped with an ApoTome.2 System (Carl Zeiss Inc., Ober Kochen, Germany). Digital images were acquired with the AxioCam MRm high resolution digital camera (Zeiss) and processed with the AxioVision 4.8.2 software (Zeiss).

2.3. Statistical analysis

Statistical analyses were performed using the software Graphpad Prism 6 (La Jolla, CA, USA).

The percentage of cell survival was assessed by one-way ANOVA, followed by Newman-Keuls post-hoc significance test. Statistical significance was defined as $p < 0.05$ (Bei et al., 2022).

3. Results and discussion

Solubility and physico-chemical properties of HA can be easily tuned by its functionalization with a wide range of molecules mainly through esterification or amidation reactions (Hintze, Schnabelrauch, & Rother, 2022). It has been shown that functionalization of HA carboxylic groups with small hydrophobic moieties can lead to the formation of amphiphilic chains, which are able to spontaneously self-assemble in water, under specific conditions of temperature and pressure (Di Meo et al., 2015; Montanari et al., 2015; Montanari et al., 2017). This event results in the formation of self-assembled NHs, which can entrap both hydrophilic and hydrophobic molecules. Indeed, it is widely known that, when a certain amount of energy is provided to such systems, the amphiphilic chains can organize themselves to maximize the inter- or intramolecular interactions among related regions and to minimize the interfacial free energy of the system (Hassan & Gawali, 2019). Thus, the hydrophobic forces that are established among the moieties grafted on the polysaccharide backbone determine the formation of internal lipophilic domains and pushes the HA chains outside, towards the aqueous medium, forming a hydrophilic shell. By properly choosing the hydrophobic moieties for HA functionalization it is also possible to provide the system with an active targeting property.

In this work, HA was chemically modified with estradiol, a female

steroid hormone belonging to the class of estrogens, which is known to play a key role in certain breast cancers. In this light, the introduction of such molecules could be useful to provide amphiphilicity to the chains and to target cells overexpressing ES receptors. Considering this, such new derivative was used to form ES-NHs which were tested as carriers of hydrophobic bioactive compounds that showed antitumoral activity towards ER+ breast cancer. Biological assays were performed to prove their ability to selectively deliver drugs to cancer cells improving their efficacy by interacting with specific receptors.

3.1. Esters of estradiol: synthetic procedure and structural analysis

ES esterification (Fig. 1A) was carried out to decrease the steric hindrance of the molecule by adding a flexible spacer, thus allowing the further reaction with HA carboxylic groups. The reaction led to the formation of an ester bond on the ES hydroxylic groups in position 3 and/or 17. Thin layer chromatography (TLC) confirmed the presence of two products: separation of the mixture and chromatographic purification of the single products allowed to calculate a 36 % yield for the first product and a 18 % yield for the second one. The identification of the products was performed by hydrogen and carbon nuclear magnetic resonance (^{1}H NMR, ^{13}C NMR, full spectra are reported in Fig. S1 and S2 of SM) and by solid state infrared spectroscopy (FTIR).

The ^{1}H NMR spectrum of 1st product (Fig. 1B, above) showed a shift of hydrogen in 17 (H_{17}) from 4.56 ppm to 4.79 ppm, compared to ES spectrum (Fig. S3 in SM), suggesting the presence of an electron withdrawing group (EWG) as the ester one. This was also confirmed by ^{13}C NMR analysis (Fig. 1B, below), where a signal at 173.09 ppm as well as a shift of C_{17} from 80.41 to 83.11 ppm referring to ES spectrum were observed.

The ^{1}H NMR spectrum of 2nd product showed the same shift of H_{17} and also additional aromatic hydrogens shift in the range of 6.9–7.4 ppm, hinting that both hydroxylic groups of ES were functionalized with an EWG (see Fig. 1C, above). Furthermore, in ^{13}C NMR spectrum the signals of the C_3 and C_{17} ester groups, at 172.50 and 171.70 ppm respectively, the shift of C_{17} from 80.41 to 82.46 ppm, as well as the shift of aromatic carbons in ortho/para-positions were clearly visible (Fig. 1C, below).

FTIR spectrum of 1st product (Fig. S4 in SM, left) showed a strong band at 1701 cm^{-1}, non-typical of ES, which was assigned to the stretching of the ester carbonyl group (ν O=C-O). In fact, Vazquez-Alcantara, Menjivar, Garcia, Diaz-Zagoya, and Garza-Flores (1989) already reported that esters of ES with long chain fatty acids were characterized by a sharp and intense signal in the range of 1710–1700 cm^{-1}. This, together with the reduction of the wide band at 3500–3000 cm^{-1}, characteristic of the stretching of the O—H bond (ν O—H), confirmed the presence of the mono-ester of ES: 17-ES-Br.

On the other hand, the sharp bands at 1751 and 1723 cm^{-1} and the lack of the wide band at 3500–3000 cm^{-1} in the FTIR spectrum of 2nd product (Fig. S4 in SM, right) were indicative of the formation of the double-ester of ES: 3,17-ES-Br.

Moreover, MS analysis on the monosubstituted 17-ES-Br product showed a m/z = 443.12, corresponding to $[C_{22}H_{29}O_3Br]Na^+$. Mass-to-charge attribution was verified by the characteristic ^{81}Br/^{79}Br isotope pattern, confirming the conjugation of ES with 4-bromobutirryl chloride.

3.2. Synthesis and FTIR-ATR characterization of HA amphiphilic derivative using 17-ES-Br as pendant group

Among all synthesized esters of ES, 17-ES-Br was selected to be the grafting moiety on the HA polymeric backbone aiming to maintain the highest receptor affinity. In fact, structure-activity relationship (SAR) studies showed that the ES relative binding affinity (RBA) with ERα and ERβ strongly decreased after the removal of the -OH in 3 (200-fold less), suggesting that the functional group in that position is essential for the interaction with the estrogenic receptors. On the other hand, changes in position 17 resulted in a lower reduction of the ES RBA (7-fold less) compared to ES (Fang et al., 2001).

Grafting of the HA backbone with 17-ES-Br moieties was performed by a S_N2 reaction in which the carboxylic group of HA repeating unit acts as a nucleophile towards the γ-carbon of 17-ES-Br leading to the formation of an ester bond (Fig. 2). To increase the solubility of the polysaccharide in organic solvents, such as NMP, the HA was used as a tetrabutylammonium salt. Thus, an additional counter-ion exchange step was required in order to replace the TBA^+ ions, which are toxic for biological systems, with the Na^+ ones. The obtained HA-ES sodium salt was then precipitated with acetone, which is a poor solvent for the polymer, and purified by extensive dialysis against water, to remove the excess of Na^+ ions and traces of organic solvents in addition to unreacted reagents.

By tuning the amount of 17-ES-Br in the reaction, HA-ES derivatives with a wide range of stoichiometric DDs were synthetized to further identify those able to promote the self-assembling in NHs in water. Specifically, a very low DD means that the hydrophobic moieties are not enough to guide the supramolecular rearrangement, whilst a too high DD leads to insoluble derivatives that are not able to self-assemble in aqueous media.

HA-ES derivatives were analysed by FTIR-ATR spectroscopy to assess the presence of the ester group, identifiable by the stretching of C=O bond between 1750 and 1700 cm^{-1}. The infrared spectrum of HA^-Na^+ (Fig. 3) showed a broad band centered at 3400 cm^{-1}, typical of the OH stretching of the sugar units, and a smaller one at 2900 cm^{-1}, related to the asymmetric and symmetric stretching of CH_2 moieties. Furthermore, an intense peak at 1600 cm^{-1}, along with a shoulder at 1550 cm^{-1}, were assigned to the asymmetric C=O stretching of carboxylic group on the D-glucuronic acid units and to the C=O stretching of amide on the *N*-acetyl-glucosamine, respectively. Finally, the symmetric stretching of carboxylate group was found at 1400 cm^{-1}, while a strong broad band centered at 1050 cm^{-1} was attributed to the C—O stretching (Leone, Consumi, Lamponi, & Magnani, 2012).

By comparing the infrared spectrum of HA^-Na^+ with those of HA-ES at different stoichiometric DDs, a specific trend was observed. Specifically, as the stoichiometric DD increased, also the peak at *ca.* 1730 cm^{-1} became more evident. This result, together with the decreasing of the intensity of the band assigned to the C=O stretching of carboxylic group, confirmed that HA was successfully functionalized with 17-ES-Br moieties *via* ester bond (Fig. 3).

3.2.1. Determination of HA-ES derivatization degree

Among all the synthesized HA-ES derivatives, those with a stoichiometric DD < 40 % were not selected due to their high water solubility. Otherwise, water dispersions of HA-ES derivatives with a stoichiometric DD ≥ 40 % resulted in opalescent suspensions, clearly confirming the amphiphilic properties of the polymers. Thus, the most homogeneous suspensions, obtained with HA-ES_{40} and HA-ES_{70}, were further investigated. Specifically, an alkaline hydrolysis was carried out to assess their DDs. In this procedure, the pH of the dispersions was increased up to 13.0 in order to promote the saponification of the ester bonds, leading to the formation of free ES and HA. After sonication, the product of the hydrolysis was extracted and quantified by HPLC at λ = 225 nm. The obtained chromatograms displayed a single and sharp peak, whose integration of the area under the curve gave a value of 501 ± 11 μg of ES for 5.0 mg of HA-ES_{40} (n = 3) and 748 ± 74 μg of ES for 5.0 mg of HA-ES_{70} (n = 2), giving a DD of 15 ± 0 % and 22 ± 2 % for HA-ES_{40} and HA-ES_{70}, respectively.

3.3. Preparation of ES-NHs and their physico-chemical characterization

The selected HA-ES_{40} and HA-ES_{70} derivatives were tested for the formation of self-assembled structures, first by magnetic stirring and then using the autoclaving process, a simple and fast strategy already

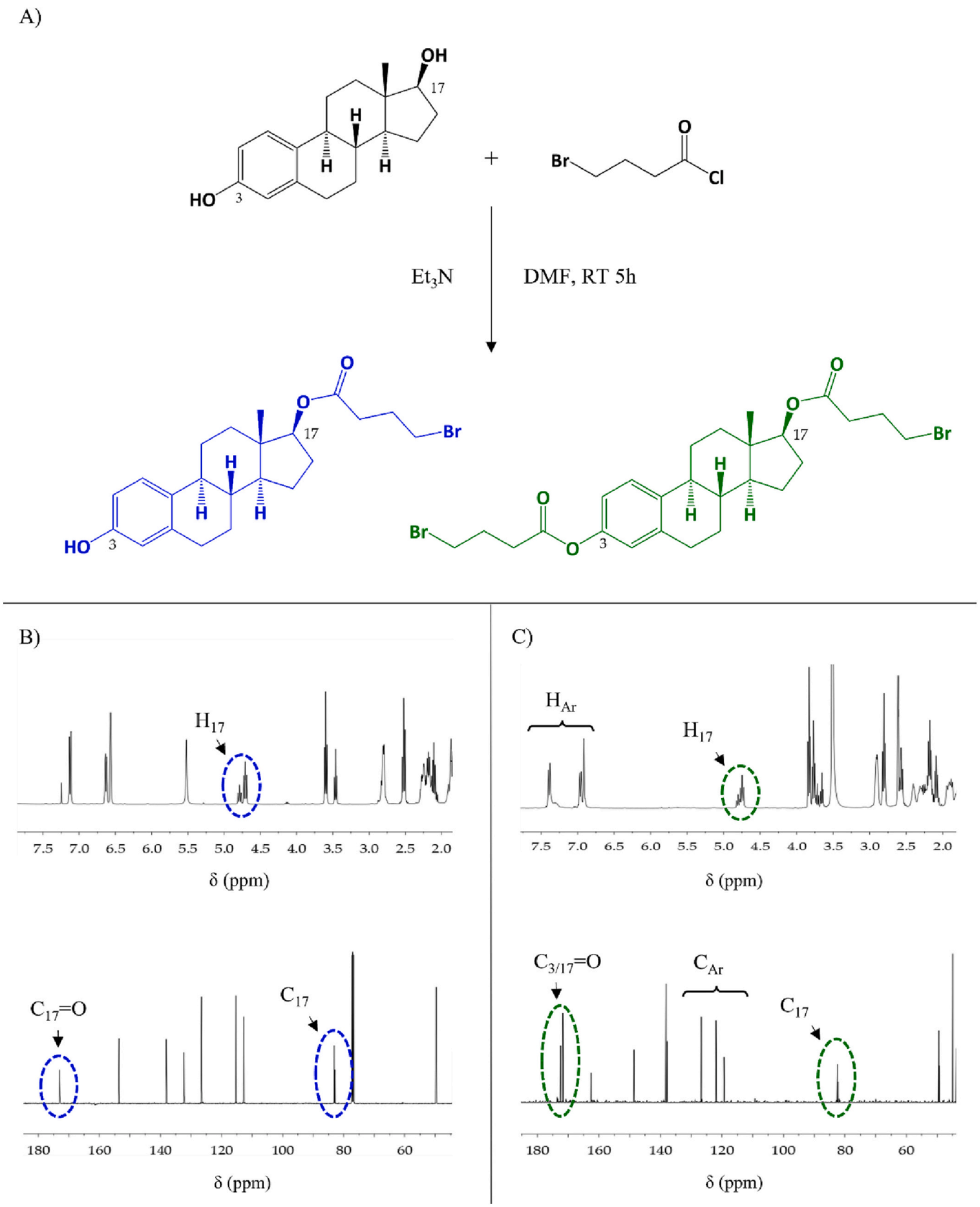

Fig. 1. A) ES esterification with 4-bromobutirryl chloride to obtain 17-ES-Br (blue) and 3,17-ES-Br (green). ^{1}H NMR (above) and ^{13}C NMR (below) spectra of B) 17-ES-Br and C) 3,17-ES-Br in which the most significant peaks are highlighted.

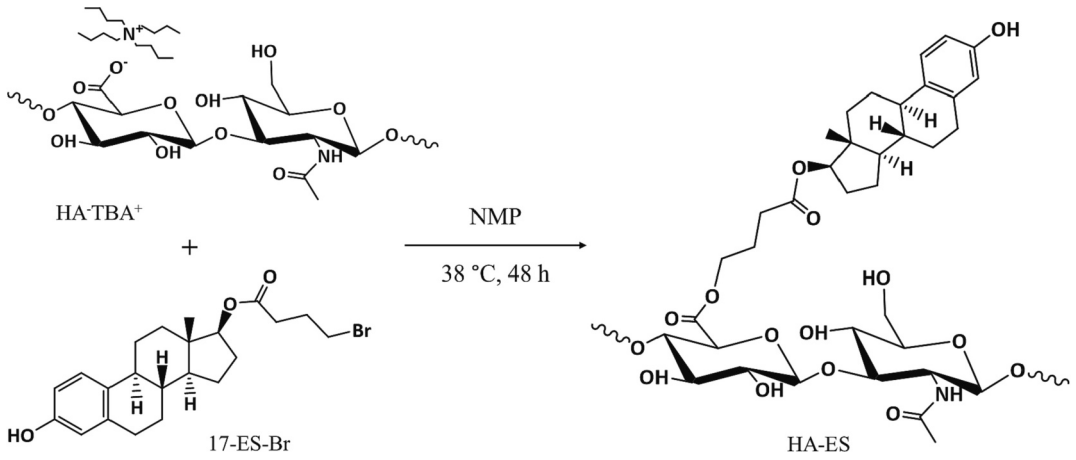

Fig. 2. Scheme of the HA grafting with 17-ES-Br to obtain an HA-ES amphiphilic derivative.

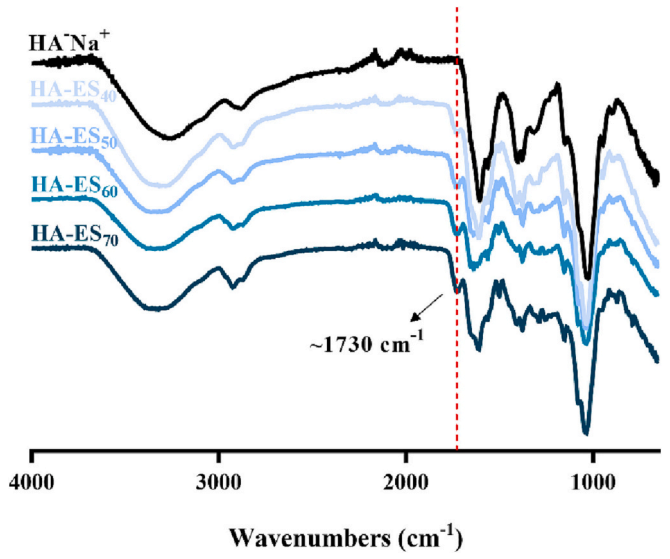

Fig. 3. FTIR-ATR spectra of HA-ES derivatives at different stoichiometric DDs: the dotted line refers to the peak at 1730 cm^{-1}, assigned to the C=O stretching of the ester functional group.

exploited for the preparation of sterile NHs based on different derivatives of hyaluronic acid (Montanari et al., 2015). For this purpose, suspensions of the two derivatives were prepared at two different concentrations, 1 and 2 mg/mL, and measured by DLS. The obtained systems showed multiple populations and size in the micrometre range, for that reason the suspensions were autoclaved at 121 °C and 1.1 bar for 20 min: these specific conditions of temperature and pressure provide the system with enough energy to allow the three-dimensional rearrangement of the amphiphilic polymer chains, which turn inward the hydrophobic moieties while expose the hydrophilic chains to the aqueous environment. We know that the autoclaving process could lead to the degradation of the polymer (Montanari et al., 2017), but we confirmed by FTIR-ATR that in our cases the structure is not affected by these specific conditions (Fig. S5 in SM). Moreover, the weight of the autoclaved polymer remains stable before and after dialysis (cut-off 12–14 kDa) excluding the presence of oligomers.

The obtained nanosystems showed an average hydrodynamic diameter of 300–400 nm, a low polydispersity index (PDI = 0.05–0.2) and a good reproducibility, hinting their potential application as drug carriers (Fig. 4A).

The ζ-potential of ES-NHs (1 mg/mL) was also measured. The ζ-potential turned out to be high and negative, as expected for the presence of many carboxylic groups on the hyaluronic chains: −33 ± 2 mV (ES-NHs_{40}) and − 36 ± 2 mV (ES-NHs_{70}). Since a stable system usually has a ζ-potential absolute value ≥30 mV, it is possible to conclude that the electrostatic repulsions established among the negatively charged nanoparticles are strong enough to prevent their aggregation.

To obtain detailed information about the storage stability of the nanosystems, ES-NHs were freeze-dried, to ensure a good long-term storage, and subsequently redispersed in water. An increasing in the hydrodynamic diameter of 20 and 50 nm for ES-NHs_{40} and ES-NHs_{70},

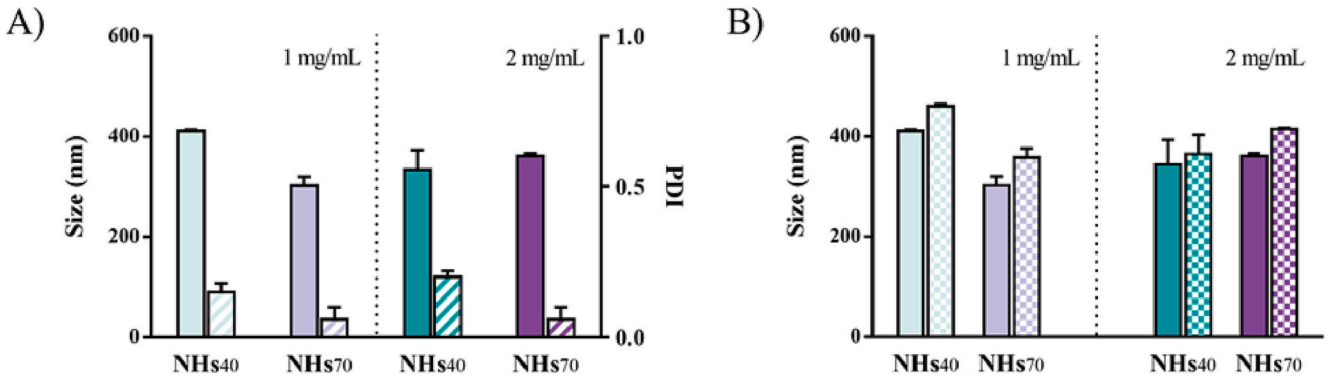

Fig. 4. A) Hydrodynamic diameter (size – full bars) and polydispersity index (PDI – striped bars) of ES-NHs_{40} and ES-NHs_{70} at 1 and 2 mg/mL; B) Stability of ES-NHs_{40} and ES-NHs_{70} before (full bars) and after (dotted bars) freeze-drying at 1 and 2 mg/mL. Data are expressed as the mean value ± standard deviation; experiments were performed in triplicate (n = 3).

respectively, was observed after the freeze-drying process (Fig. 4B). These results strongly encourage the use of the freeze-drying to store the NHs in a safer and long-lasting way, ready to be used when needed.

However, further studies of both suspensions over time (data not shown) led to the choice of ES-NHs$_{40}$ 1 mg/mL (hereafter called just ES-NHs) for a more in-depth investigation and the following experiments.

Ultrastructural TEM analysis of ES-NHs$_{40}$ showed the presence of nano-sized, rounded-shaped particles with a size ranging between 120 and 250 nm (Fig. 5).

3.4. Formulations of ES-NHs with bioactive molecules

In order to assess whether these nanosystems could act as smart carriers for drug delivery purposes, the loading capability of ES-NHs was tested. Two different molecules were selected, CUR and DTX, which were loaded with different techniques according to their physico-chemical properties, such as solubility and thermal stability. In fact, while CUR could be loaded into ES-NHs during their formation process using the autoclave at 121 °C, DTX is not a thermostable molecule, and it was loaded into already formed ES-NHs by contact with a dry DTX film at 40 °C (Fig. 6).

3.4.1. ES-NHs/CUR formulation and characterization

CUR, a mixture of three natural antioxidant molecules with a low water solubility and already loaded into a similar polysaccharide-based platform (Montanari et al., 2019), was used as a hydrophobic model molecule to demonstrate that ES-NHs can be a suitable carrier for the delivery of hydrophobic and easily degradable biomolecules. According to the procedures reported above (Section 2.2.5), HA-ES$_{40}$ suspensions were added to CUR films and kept in autoclave at 121 °C for 20 min to allow the formation of the nanosystems (Fig. 6A). The purification of the ES-NHs/CUR from the unloaded molecule led to an %EE of 67.0 ± 3.0, and a %DL of 22.0 ± 1.0, corresponding of 220 μg of CUR *per* mg of HA-ES, as confirmed by HPLC. As result, the apparent water solubility of CUR was increased by 70 times compared to its nominal solubility in water (3 μg/mL). This could be ascribed to the establishment of hydrophobic forces between CUR and ES moieties of the NHs.

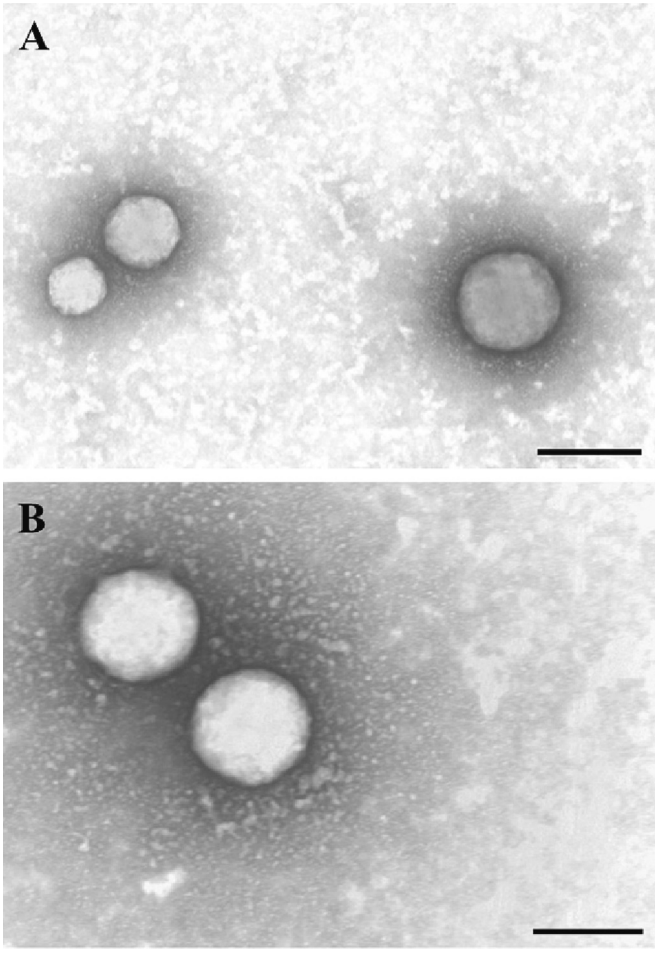

Fig. 5. Ultrastructural analysis of ES-NHs$_{40}$. Representative images of ES-NHs at lower (A) and higher magnification (B) are reported. Nano-sized, rounded-shaped particles are visible. Bars correspond to 200 nm.

Physico-chemical characterization of ES-NHs/CUR was performed by means of DLS with the assessment of the hydrodynamic diameter, PDI and ζ-potential: the systems showed an average hydrodynamic diameter of 232 ± 29 nm and a low polydispersity (PDI = 0.1). The smaller size of ES-NHs/CUR, compared to the empty ones, can be ascribed to the presence of CUR which contributes to the establishment of hydrophobic forces in the inner NHs hydrophobic domains, with the formation of more compact structures. The ζ-potential value of the formulation remained high and negative (−35 ± 2 mV), hence preventing the aggregation during the time. In the light of a long-term storage, such nanosystems were also tested after freeze-drying, showing an increase of their hydrodynamic dimensions of *ca.* 100 nm reaching about 330 nm in size and resulting stable over time (data not shown).

As a support for the following *in vitro* studies, the stability of ES-NHs/CUR was also evaluated in simulated physiological conditions, by adding phosphate-buffered saline (PBS) at pH = 7.4 and glycerol to reach a final concentration of 1 mM and 2 % w/V, respectively. Since the nanoformulation was stable in these conditions (Fig. S6 in SM), the system was further investigated *in vitro*.

3.4.1.1. In tube antioxidant activity of ES-NHs/CUR formulations. After the preparation of loaded and stable ES-NHs/CUR formulations, the antioxidant activity of CUR was tested in order to verify that the loaded molecule could maintain its activity inside the nanosystems. For that reason, ABTS test was performed, and the antioxidant activity of the formulations was compared to that of the free molecule. The ABTS assay is based on the generation of a radical cation ($ABTS^{\bullet+}$) by reaction of ABTS with a strong oxidising agent and measures the ability of a molecule to act as a scavenger by turning off the $ABTS^{\bullet+}$ (Amorati & Valgimigli, 2015).

The kinetics of the antioxidant activity was evaluated by adding the sample under investigation to the $ABTS^{\bullet+}$ solution and monitoring the absorbance trend at 730 nm for 30 min. CUR solution in AcCN, at a concentration equal to the amount loaded into NHs, was also tested as a control. The results showed that even the unloaded ES-NHs (which were used as blanks), had a radical scavenging activity thanks to the presence of ES. Indeed, it is well known that the phenolic group, which is linked to the ring A of the gonan nucleus of estrogens, is able to extinguish the free radicals by transferring an H^+ atom to a peroxyl radical, forming more stable radical species (Chiorcea-Paquim, Enache, Gil, & Oliveira-Brett, 2020). As reported in Fig. S7 (see SM), ES-NHs/CUR performed a higher antioxidant activity compared to that of empty NHs and free CUR, suggesting a synergic effect between ES and CUR.

Considering the absorbance values at 6, 12 and 30 min, the antioxidant activity (%A) of CUR in ES-NHs and its increase compared to free CUR (%IA) were calculated according to Eqs. (4) and (5) (Section 2.2.6). It appeared that the loaded formulation had a higher %A than free CUR and empty NHs for the same time points. As a result, the antioxidant activity of CUR significantly increased when the molecule was loaded into the nanoparticles: %IA of 35, after 30 min of incubation (Fig. 7A). This result may be due to two factors: the presence of ES and the enhancement of the water-solubility of CUR, which can therefore better interact with the ABTS radicals.

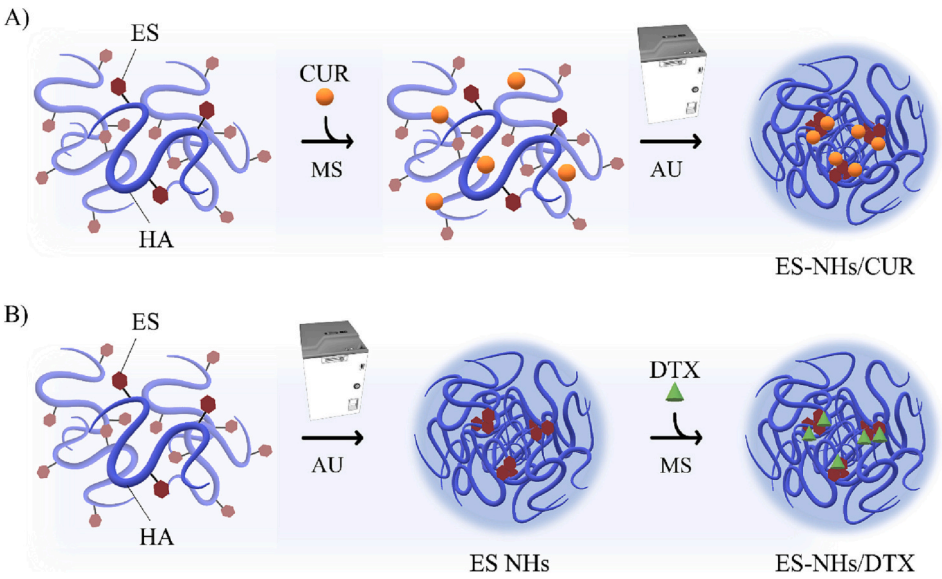

Fig. 6. Schematic representation of ES-NHs/CUR (A) and ES-NHs/DTX (B) formulation by autoclaving treatment. MS: magnetic stirring; AU: autoclave.

A)

	%A	%IA	%A	%IA	%A	%IA
	t = 6 min		t = 12 min		t = 30 min	
Free CUR	36 ± 3		40 ± 2		46 ± 2	
ES-NHs	35 ± 5		41 ± 6		49 ± 8	
ES-NHs/CUR	47 ± 1	31 ± 4	53 ± 2	33 ± 4	62 ± 2	35 ± 4

B)

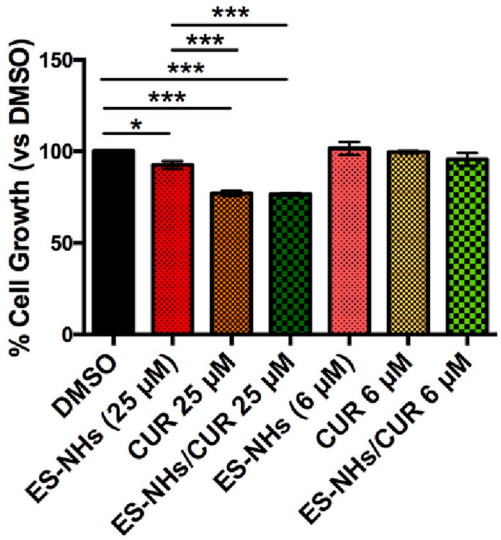

Fig. 7. A) Antioxidant activity (%A) and increased antioxidant activity (%IA) of ES-NHs and ES-NHs/CUR recorded after 6, 12 and 30 min of incubation. For an appropriate comparison, the data relative to free CUR are also reported. B) Effect of ES-NHs/CUR, ES-NHs and CUR on MCF-7 cell line. The MCF-7 cell growth was assessed by the SRB assay after 48 h of treatment and the growth rate of cells was calculated in comparison with that of control cells treated with DMSO 0.01 % V/V. The results are expressed as the mean ± standard deviation (SD) of three independent experiments performed in triplicate. (*$p < 0.05$, **$p < 0.01$, *** $p < 0.001$ *vs* DMSO).

3.4.1.2. In vitro effects of ES-NHs/CUR, ES-NHs, CUR on MCF-7 cells survival. Sulforhodamine B (SRB) assay was used to investigate cell proliferation by measuring the cellular protein content of adherent cell cultures. SRB is a dye able to stoichiometric bind basic aminoacids under mild acidic conditions and dissociate under basic conditions (Vichai & Kirtikara, 2006). The proliferation of the estrogen receptor ER+ human breast cancer cell line, MCF-7, was evaluated by the SRB assay after their incubation with increasing concentrations of ES-NHs/CUR, ES-NHs and CUR (6–25 μM) for 48 h. DMSO 0.01 % V/V was used as control and empty ES-NHs were used at the same concentrations needed for the treatments with ES-NHs/CUR 6 μM or 25 μM. Our results demonstrated that ES-NHs/CUR treatment inhibited MCF-7 cells growth in a dose-dependent manner when compared to ES-NHs (Fig. 7B). No differences were observed between ES-NHs/CUR, CUR and ES/NHs treatments at the concentration of 6 μM; on the other hand, ES-NHs/CUR significantly inhibited cells proliferation at a concentration of 25 μM

when compared to DMSO-treated cells ($p < 0.001$) or ES-NHs ($p < 0.001$). The same level of growth inhibition was obtained using CUR as free drug, even though it required to be solubilized in DMSO.

Overall, the use of this nanogel platform for loading and delivering CUR as a hydrophobic model molecule provides cells growth inhibition, thus representing a promising approach to improve the solubility of poorly water-soluble drugs, including CUR – and therefore facilitate their local and systemic administration – and ensure protection from the environment for the most unstable ones.

3.4.2. ES-NHs/DTX formulation and characterization

Once verified the possibility to use ES-NHs as nanocarriers able to efficiently load bioactive molecules, increasing their water-solubility and retaining their activity, an anticancer drug was used in order to study the active targeting towards cells that overexpressed HA and/or ES receptors on their surfaces and nuclei, like the ER+ breast cancer cells. Docetaxel (DTX), which belongs to the chemotherapy class of taxane, is one of the most effective drugs against breast cancer. However, it is characterized by a very poor solubility in water (logP = 4.1) and serious side effects that strongly limit its use (Montero, Fossella, Hortobagyi, & Valero, 2005). Thus, the idea of using such ES-NHs to encapsulate and deliver DTX in a site-specific manner could be a very promising strategy to overcome the mentioned drawbacks.

Loading of DTX into ES-NHs was achieved by magnetic stirring: a DTX film was hydrated with a 1 mg/mL ES-NHs suspension at 40 °C for 15 h. In this case, the autoclave was used only for the formation of the empty ES-NHs due to the thermal instability of DTX at high temperatures (Fig. 6B). Centrifugation of ES-NHs/DTX allowed to recover the unloaded drug, which was quantified by HPLC to determine the EE and DL percentage. DTX was loaded with an %EE of 12.0 ± 1.0 % and a %DL of 4.0 ± 0.1 %, reaching a concentration of 40 μg/mL. The amount of entrapped drug led to a water solubility of 6–7 times higher than that of the free DTX (about 6 μg/mL), suggesting that loading a compound into an already-formed structure is more challenging than a one step procedure in which the molecule is added during the formation of the nanosystem. ES-NHs/DTX formulation had an average hydrodynamic diameter of 342 ± 23 nm and a PDI of 0.20 ± 0.02, supporting even more the idea that, the presence of the drug during the rearrangement of the polymeric chains, plays a key role in the formation of more cohesive structures.

3.4.2.1. In vitro effects of ES-NHs/DTX, ES-NHs and DTX on MCF-7 cells survival. The proliferation of the MCF-7 cell line was evaluated by the SRB assay after exposure to increasing concentrations of ES-NHs/DTX, ES-NHs and DTX (12.5–50 μM) for 48 h. DMSO 0.01 % V/V was used as control and empty ES-NHs were used at the same concentrations needed for the treatments with ES-NHs/DTX 12.5 μM and 50 μM. Our results demonstrated that ES-NHs/DTX treatment inhibited MCF-7 cells growth when compared to ES-NHs (Fig. 8), but the ability to inhibit cells growth by ES-NHs/DTX was higher than that by DTX for both the investigated concentrations after 48 h of treatment.

In addition, a significant inhibition of cell growth in cells treated with ES-NHs/DTX at a concentration of 50 μM and 12.5 μM when compared to DMSO ($p < 0.01$ and $p < 0.001$ respectively), ES-NHs ($p < 0.001$) and DTX ($p < 0.05$ and $p < 0.001$ respectively) after 48 h of treatment was observed. There is no difference between the effect of DTX alone at the concentration of 12.5 μM or 50 μM. Similarly, no significant difference was observed between the effect of ES-NHs/DTX at the concentration of 12.5 μM or 50 μM. Moreover, ES-NHs treatment did not show toxic effects on the human breast cancer cell line.

This observation suggests that such nanosystems are really effective in conveying the drug to the target site, resulting in a greater pharmacological effect with the same dose.

We can assume that the encapsulation of DTX into ES-NHs can improve its solubility, protect the drug from the degradation, and also enable its delivery towards ER+ cancer cells thanks to the recognition of specific receptors expressed on the cell surface by the ES-NHs. The stronger activity of ES-NHs/DTX formulation – with respect to the free drug – could be ascribed to an internalization of the loaded nanosystems, mediated by mERs or CD44 receptors, hence resulting in a higher concentration of DTX inside the cells. Finally, since ES receptors are mainly located in the cell nuclei, a nuclear active targeting could even be further deepened exploiting cytotoxic drugs with a nuclear activity.

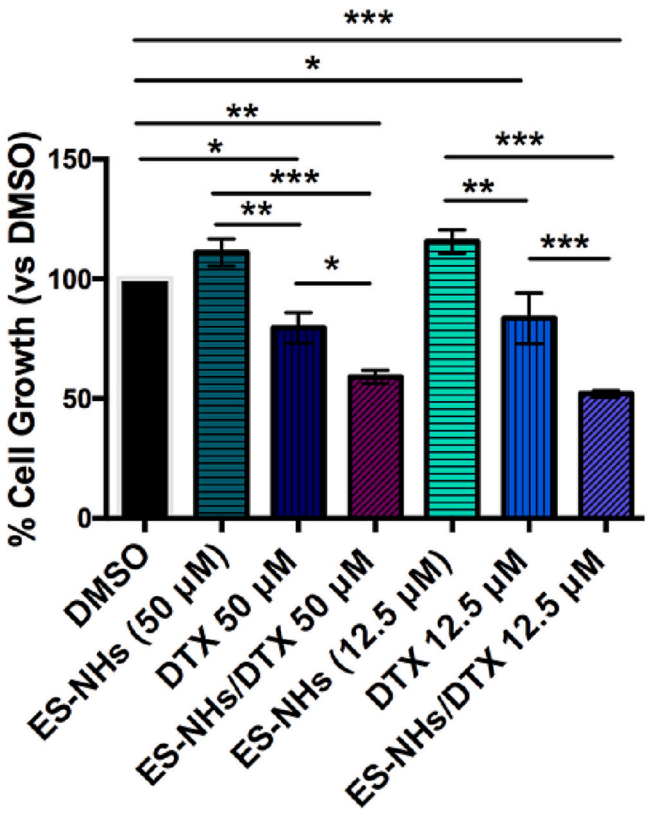

Fig. 8. Effect of ES-NHs/DTX, ES-NHs and DTX on MCF-7 cell line. The MCF-7 cell growth was assessed by the SRB assay after 48 h of treatment with ES-NHs/DTX, ES-NHs and DTX or DMSO. The growth rate of cells treated with ES-NHs/DTX, ES-NHs and DTX was calculated in comparison with that of control cells treated with DMSO 0.01 % V/V. The results are expressed as the mean ± standard deviation (SD) of three independent experiments performed in triplicate. (*$p < 0.05$, **$p < 0.01$, *** $p < 0.001$ *vs* DMSO).

3.5. Internalization experiments

Fluorescent ES-NHs were prepared by linking Rhod to the HA-ES_{40} derivative, as reported in the Section 2.2.8 and in Fig. S8 in SM. The resulting derivative Rhod-HA-ES retained its ability to form NHs (Rhod-ES-NHs), with a mean hydrodynamic diameter of 336 nm and a PDI of 0.30.

We evaluated the ability of Rhod-ES-NHs to enter MCF-7 cells through *in vitro* uptake experiments and subsequent evaluation by fluorescence techniques. ApoTome images showed that after 30 min of internalization, the Rhod-ES-NHs were distributed inside the cells in vesicle-like structures, located partly near the cell membrane and partly near the nuclei (Fig. 9), suggesting a rapid intracellular uptake of Rhod-ES-NHs.

4. Conclusions

Polysaccharide-based nanoparticles have been widely studied as efficient and versatile carriers for several biomedical applications: from

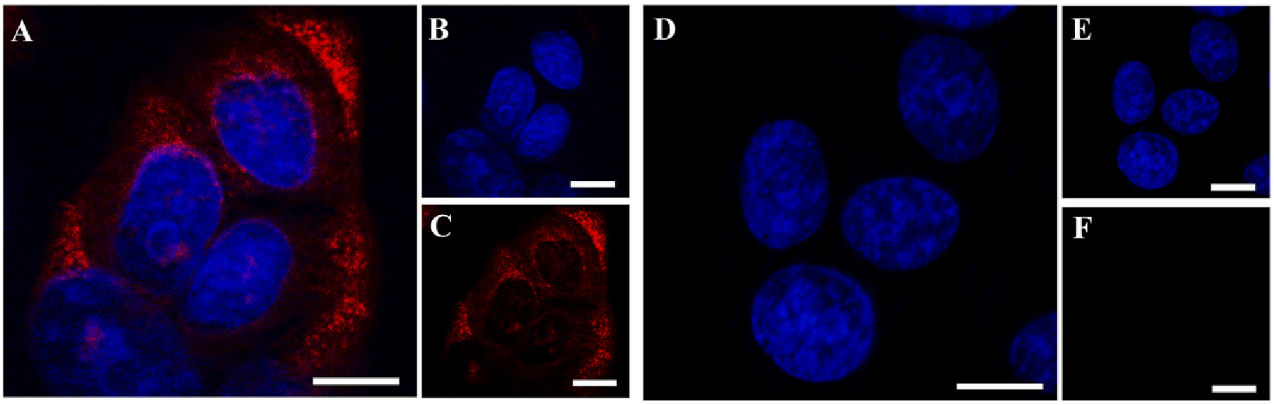

Fig. 9. Fluorescence analysis of MCF-7 cells incubated with fluorescent Rhod-ES-NHs for 30 min: A) merge, B) DAPI, C) Rhod-ES-NHs; D) merge, E) DAPI, F) free Rhod. Bars correspond to 20 μm.

anticancer and antimicrobial therapy to vaccines and nucleic acids delivery for gene therapy. However, to the best of our knowledge, only liposomes, dendrimers and synthetic polymeric nanoparticles have been functionalized with estrogens to actively target hormone-sensitive tumors, such as breast cancer.

The new platform described here is based on the chemical conjugation of HA with ES, through the introduction of a linear spacer, which resulted in an amphiphilic derivative able to spontaneously self-assemble in water. A proper derivatization degree allowed to obtain self-assembled, sterile, and small-sized nanogels (ES-NHs) which can be used as carriers for the delivery of hydrophobic drugs. CUR and DTX were encapsulated into ES-NHs and their activity in inhibiting the growth of the ER+ breast cancer cell line MCF-7 was evaluated. While ES-NHs had not toxic effects on the cells, both ES-NHs/CUR and ES-NHs/DTX treatment inhibited MCF-7 cell growth and ES-NHs/DTX effect was statistically higher than that of free DTX. Moreover, fluorescent Rhod-ES-NHs showed to be rapidly internalized into MCF-7 cells and localized near cell and nuclear membranes. These results indicate that ES-NHs are suitable systems to deliver the drugs into ER+ cancer cells, assuming a receptor-mediated internalization and targeting.

CRediT authorship contribution statement

L. Paoletti: Investigation, Validation, Resources, Data curation, Writing – original draft. **N. Zoratto:** Investigation, Validation, Resources, Data curation, Writing – review & editing. **M. Benvenuto:** Investigation, Validation, Resources, Data curation, Writing – original draft. **D. Nardozi:** Investigation, Validation, Resources, Data curation. **V. Angiolini:** Investigation, Validation, Resources, Data curation. **P. Mancini:** Investigation, Validation, Resources, Data curation. **L. Masuelli:** Methodology, Supervision, Validation, Data curation, Writing – review & editing. **R. Bei:** Methodology, Supervision, Validation, Funding acquisition, Writing – review & editing. **G.V. Frajese:** Conceptualization, Methodology, Supervision, Project administration. **P. Matricardi:** Methodology, Supervision, Validation, Project administration, Funding acquisition, Writing – review & editing. **M. Nalli:** Methodology, Supervision, Validation, Project administration, Data curation, Writing – review & editing. **C. Di Meo:** Conceptualization, Methodology, Supervision, Validation, Project administration, Funding acquisition, Writing – review & editing.

Declaration of competing interest

The authors declare that they have no known competing financial interests or personal relationships that could have appeared to influence the work reported in this paper.

Data availability

Data will be made available on request.

Acknowledgements

This work was supported by Sapienza University of Rome "Finanziamenti di Ateneo per la Ricerca Scientifica – RM120172AE742B3B (Di Meo C.) and RM12117A81AEF242 (Matricardi P.). Grant from Ministero dell'Università e della Ricerca, PRIN (BeiR20Prin, CUP: E85F22000060006 to R.B.) is also acknowledged (Bei R.).

Appendix A. Supplementary data

Supplementary data to this article can be found online at https://doi.org/10.1016/j.carbpol.2023.120900.

References

Acconcia, F., Fiocchetti, M., Busonero, C., Fernandez, V. S., Montalesi, E., Cipolletti, M., Pallottini, V., & Marino, M. (2021). The extra-nuclear interactome of the estrogen receptors: Implications for physiological functions. *Molecular and Cellular Endocrinology, 538*, 111452.

Acconcia, F., & Marino, M. (2011). The effects of 17β-estradiol in cancer are mediated by estrogen receptor signaling at the plasma membrane. *Frontiers in Physiology, 2*, 30.

Amorati, R., & Valgimigli, L. (2015). Advantages and limitations of common testing methods for antioxidants. *Free Radical Research, 49*(5), 633–649.

Bei, R., Benvenuto, M., Focaccetti, C., Fazi, S., Moretti, M., Nardozi, D., Angiolini, V., Ciuffa, S., Cifaldi, L., Carrano, R., Palumbo, C., Miele, M. T., Bei, R., Barillari, G., Manzari, V., De Smaele, E., Modesti, A., & Masuelli, L. (2022). Combined treatment with inhibitors of ErbB receptors and hh signaling pathways is more effective than single treatment in reducing the growth of malignant mesothelioma both in vitro and in vivo. *Journal of Translational Medicine, 20*(1), 286.

Benvenuto, M., Ciuffa, S., Focaccetti, C., Sbardella, D., Fazi, S., Scimeca, M., Tundo, G. R., Barillari, G., Segni, M., Bonanno, E., Manzari, V., Modesti, A., Masuelli, L., Coletta, M., & Bei, R. (2021). Proteasome inhibition by bortezomib parallels a reduction in head and neck cancer cells growth, and an increase in tumor-infiltrating immune cells. *Scientific Reports, 11*(1), 19051.

Boonyaratanakornkit, V., Hamilton, N., Márquez-Garbán, D. C., Pateetin, P., McGowan, E. M., & Pietras, R. J. (2018). Extranuclear signaling by sex steroid receptors and clinical implications in breast cancer. *Molecular and Cellular Endocrinology, 466*, 51–72.

Chiorcea-Paquim, A.-M., Enache, T. A., Gil, E. S., & Oliveira-Brett, A. M. (2020). Natural phenolic antioxidants electrochemistry: Towards a new food science methodology. *Comprehensive Reviews in Food Science and Food Safety, 19*, 1680–1726.

Curcio, M., Vittorio, O., Bell, J. L., Iemma, F., Nicoletta, F. P., & Cirillo, G. (2022). Hyaluronic acid within self-assembling nanoparticles: Endless possibilities for targeted cancer therapy. *Nanomaterials, 12*(16), 2851.

Di Meo, C., Montanari, E., Manzi, L., Villani, C., Coviello, T., & Matricardi, P. (2015). Highly versatile nanohydrogel platform based on riboflavin-polysaccharide derivatives useful in the development of intrinsically fluorescent and cytocompatible drug carriers. *Carbohydrate Polymers, 115*, 502–509.

Fallacara, A., Baldini, E., Manfredini, S., & Vertuani, S. (2018). Hyaluronic acid in the third millenium. *Polymers, 10*(7), 701.

Fang, H., Tong, W., Shi, L. M., Blair, R., Perkins, R., Branham, W., Hass, B. S., Xie, Q., Dial, S. L., Moland, C. L., & Sheehan, D. M. (2001). Structure-activity relationships

for a large diverse set of natural, synthetic, and environmental estrogens. *Chemical Research in Toxicology, 14*(3), 280–294.
Focaccetti, C., Benvenuto, M., Ciuffa, S., Fazi, S., Scimeca, M., Nardi, A., Miele, M. T., Battisti, A., Bonanno, E., Modesti, A., Masuelli, L., & Bei, R. (2020). Curcumin enhances the antitumoral effect induced by the recombinant vaccinia neu vaccine (rV-neuT) in mice with transplanted salivary gland carcinoma cells. *Nutrients, 12*(5), 1417.
Fuentes, N., & Silveyra, P. (2019). Estrogen receptor signaling mechanisms. *Advances in Protein Chemistry and Structural Biology, 2019*(116), 135–170.
Giordano, A., & Tommonaro, G. (2019). Curcumin and cancer. *Nutrients, 11*(10), 2376.
Guo, J., Lin, W., Weng, Y., Chen, Y., Zeng, S., Lin, J., Zheng, X., Li, X., Lin, M., Yu, X., & Chen, Q. (2022). Optimal exposure to docetaxel in adjuvant chemotherapy for early-stage breast cancer. *Journal of Clinical Pharmacy and Therapeutics, 47*(12), 2205–2213.
Hassan, P. A., & Gawali, S. L. (2019). Directing amphiphilic self-assembly: From microstructure control to interfacial engineering. *Langmuir, 35*, 9635–9646.
Hintze, V., Schnabelrauch, M., & Rother, S. (2022). Chemical modification of hyaluronan and their biomedical applications. *Frontiers in Chemistry, 10*, 830671.
Jain, S., Spandana, G., Agrawal, A. K., Kushwah, V., & Thanki, K. (2015). Enhanced antitumor efficacy and reduced toxicity of docetaxel loaded estradiol functionalized stealth polymeric nanoparticles. *Molecular Pharmaceutics, 12*(11), 3871–3884.
Johansson, Å., Schmitz, D., Höglund, J., Hadizadeh, F., Karlsson, T., & Ek, W. E. (2022). Investigating the effect of estradiol levels on the risk of breast, endometrial, and ovarian cancer. *Journal of the Endocrine Society, 6*(8).
Kabanov, A. V., & Vinogradov, S. V. (2009). Nanogels as pharmaceutical carriers: Finite networks of infinite capabilities. *Angewandte Chemie International Edition, 48*(30), 5418–5429.
Kampa, M., Pelekanou, V., & Castanas, E. (2008). Membrane-initiated steroid action in breast and prostate cancer. *Steroids, 73*(9–10), 953–960.
Khan, M. Z. I., Uzair, M., Nazli, A., & Chen, J. Z. (2022). An overview on estrogen receptors signaling and its ligands in breast cancer. *European Journal of Medicinal Chemistry, 241*, 114658.
Leone, G., Consumi, M., Lamponi, S., & Magnani, A. (2012). New hyaluronan derivative with prolonged half-life for ophthalmological formulation. *Carbohydrate Polymers, 88*(3), 799–808.
Marczell, I., Balogh, P., Nyiro, G., Kiss, A. L., Kovacs, B., Bekesi, G., Racz, K., & Patocs, A. (2018). Membrane-bound estrogen receptor alpha initiated signaling is dynamin dependent in breast cancer cells. *European Journal of Medical Research, 23*, 31.
Masuelli, L., Marzocchella, L., Focaccetti, C., Tresoldi, I., Palumbo, C., Izzi, V., Benvenuto, M., Fantini, M., Lista, F., Tarantino, U., Modesti, A., Galvano, F., & Bei, R. (2012). Resveratrol and diallyl disulfide enhance curcumin-induced sarcoma cell apoptosis. *Frontiers in Bioscience, 17*, 498–508.
Mattheolabakis, G., Milane, L., Singh, A., & Amiji, M. M. (2015). Hyaluronic acid targeting of CD44 for cancer therapy: From receptor biology to nanomedicine. *Journal of Drug Targeting, 23*(7–8), 605–618.
Mazdaei, M., & Asare-Addo, K. (2022). A mini-review of nanocarriers in drug delivery systems. *British Journal of Pharmacy, 7*(1), 1–13.
Montanari, E., Capece, S., Di Meo, C., Meringolo, M., Coviello, T., Agostinelli, E., & Matricardi, P. (2013). Hyaluronic acid nanohydrogels as a useful tool for BSAO immobilization in the treatment of melanoma cancer cells. *Macromolecular Bioscience, 13*(9), 1185–1194.
Montanari, E., De Rugeriis, M. C., Di Meo, C., Censi, R., Coviello, T., Alhaique, F., & Matricardi, P. (2015). One-step formation and sterilization of gellan and hyaluronan nanohydrogels using autoclave. *Journal of Materials Science: Materials in Medicine, 26, Article 32*.
Montanari, E., Di Meo, C., Coviello, T., Gueguen, V., Pavon-Djavid, G., & Matricardi, P. (2019). Intracellular delivery of natural antioxidants via hyaluronan nanohydrogels. *Pharmaceutics, 11*(10), 532.
Montanari, E., Di Meo, C., Oates, A., Coviello, T., & Matricardi, P. (2018). Pursuing intracellular pathogens with hyaluronan. From a 'pro-infection' polymer to a biomaterial for 'Trojan horse' systems. *Molecules, 23*(4), 939.
Montanari, E., Di Meo, C., Sennato, S., Francioso, A., Marinelli, A. L., Ranzo, F., Svhippa, S., Coviello, T., Bordi, F., & Matricardi, P. (2017). Hyaluronan-cholesterol nanohydrogels: Characterisation and effectiveness in carrying alginate lyase. *New Biotechnology, 37*, 80–89.
Montero, A., Fossella, F., Hortobagyi, G., & Valero, V. (2005). Docetaxel for treatment of solid tumours: A systematic review of clinical data. *The Lancet Oncology, 6*(4), 229–239.
Paliwal, S. R., Paliwal, R., Agrawal, G. P., & Vyas, S. P. (2012). Targeted breast cancer nanotherapeutics: Options and opportunities with estrogen receptors. *Critical Reviews™ in Therapeutic Drug Carrier Systems, 29*(5), 421–446.
Patra, J. K., Das, G., Fraceto, L. F., Ramos Campos, E. V., Rodriguez-Torres, M. P., Acosta-Torres, L. S., Diaz-Torres, L. A., Grillo, R., Swamy, M. K., Sharma, S., Habtemariam, S., & Shin, H. S. (2018). Nano based drug delivery systems: Recent developments and future prospects. *Journal of Nanobiotechnology, 16*, 71.
Plucinski, A., Lyu, Z., & Schmidt, B. V. K. J. (2021). Polysaccharide nanoparticles: From fabrication to applications. *Journal of Materials Chemistry B, 9*(35), 7030–7062.
Quagliarini, E., Renzi, S., Digiacomo, L., Giulimondi, F., Sartori, B., Amenitsch, H., Masuelli, L., Bei, R., Cui, L., Wang, J., Amici, A., Marchini, C., Pozzi, D., Caracciolo, G., & Tassinari, V. (2021). Microfluidic formulation of DNA-loaded multicomponent lipid nanoparticles for gene delivery. *Pharmaceutics, 13*(8), 1292.
Sanità, G., Carrese, B., & Lamberti, A. (2020). Nanoparticle surface functionalization: How to improve biocompatibility and cellular internalization. *Frontiers in Molecular Biosciences, 7*, 587012.
Senapati, S., Mahanta, A. K., Kumar, S., & Maiti, P. (2018). Controlled drug delivery vehicles for cancer treatment and their performance. *Signal Transduction and Targeted Therapy, 3*, 7.
Škubník, J., Pavlíčková, V., Ruml, T., & Rimpelová, S. (2021). Current perspectives on taxanes: focus on their bioactivity, delivery and combination therapy. *Plants (Basel), 10*(3), 569.
Swain, S. M., Baselga, J., Kim, S.-B., Ro, J., Semiglazov, V., Campone, M., , … Cortés, J., & CLEOPATRA Study Group. (2020). Pertuzumab, trastuzumab, and docetaxel in HER2-positive metastatic breast cancer. *The New England Journal of Medicine, 372*(8), 724–734.
Tammam, S. N., Azzazy, H. M. E., & Lamprecht, A. (2016). How successful is nuclear targeting by nanocarriers? *Journal of Controlled Release, 229*, 140–153.
Tecalco-Cruz, A. C., Macías-Silva, M., Ramírez-Jarquín, J. O., & Ramírez-Jarquín, U. N. (2022). Decoding the therapeutic implications of the ERα stability and subcellular distribution in breast cancer. *Frontiers in Endocrinology, 13*, 867448.
Vargason, A. M., Anselmo, A. C., & Mitragotri, S. (2021). The evolution of commercial drug delivery technologies. *Nature Biomedical Engineering, 5*, 951–967.
Vazquez-Alcantara, M. A., Menjivar, M., Garcia, G. A., Diaz-Zagoya, J. C., & Garza-Flores, J. (1989). Long-acting estrogenic responses of estradiol fatty acid esters. *Journal of Steroid Biochemistry, 33*(6), 1111–1118.
Vichai, V., & Kirtikara, K. (2006). Sulforhodamine B colorimetric assay for cytotoxicity screening. *Nature Protocols, 1*(3), 1112–1116.
Waks, A. G., & Winer, E. P. (2019). Breast cancer treatment: A review. *JAMA, 321*(3), 288–300.
Weissmann, B., & Meyer, K. (1954). The structure of hyalobiuronic acid and of hyaluronic acid from umbilical cord. *Journal of the American Chemistry Society, 76*, 1753–1757.
Zoratto, N., Forcina, L., Matassa, R., Mosca, L., Familiari, G., Musarò, A., Mattei, M., Coviello, T., Di Meo, C., & Matricardi, P. (2021). Hyaluronan-cholesterol nanogels for the enhancement of the ocular delivery of therapeutics. *Pharmaceutics, 13*(11), 1781.